

Spin-polarization coupling in multiferroic transition-metal oxides

Chenglong Jia,^{1,*} Shigeki Onoda,^{2,†} Naoto Nagaosa,^{2,3,‡} and Jung Hoon Han^{4,5,§}

¹*School of Physics, Korea Institute for Advanced Study, Seoul 130-012, Korea*

²*CREST, Department of Applied Physics, University of Tokyo, Tokyo 113-8656, Japan*

³*Correlation Electron Research Center, National Institute of Advanced*

Industrial Science and Technology, 1-1-1, Higashi, Tsukuba 305-8562, Japan

⁴*Department of Physics and Institute for Basic Science Research,*

Sungkyunkwan University, Suwon 440-746, Korea

⁵*CSCMR, Seoul National University, Seoul 151-747, Korea*

(Dated: July 19, 2021)

A systematic microscopic theory of magnetically induced ferroelectricity and lattice modulation is presented for all electron configurations of Mott-insulating transition-metal oxides. Various mechanisms of polarization are identified in terms of a strong-coupling perturbation theory. Especially, the spin-orbit interaction acting on the ligand p orbitals is shown to give the ferroelectric polarization of the spin-current form, which plays a crucial role particularly in e_g systems. Semiquantitative agreements with the multiferroic TbMnO_3 are obtained. Predictions for X-ray and neutron scattering experiments are proposed to clarify the microscopic mechanism of the spin-polarization coupling in different materials.

PACS numbers: 75.80.+q, 71.70.Ej, 77.80.-e

The coupling among the charge, spin, and orbital degrees of freedom in Mott insulators has been one of the central issues in strongly correlated electron systems. Despite the charge localization, its displacement can occur accompanied by the lattice deformation as in the dielectric or ferroelectric band insulators. In the case of Mott insulators, the charge displacement is usually triggered by a non-trivial low-energy spin and/or orbital structure, which is unveiled within an energy scale of the exchange interaction $J \sim V^4/\Delta^3$ with the hybridization V and the charge transfer energy Δ between the transition-metal (TM) d and ligand (L) p orbitals. There, the ferroelectricity and the magnetism sometimes appear concomitantly as a spontaneous magnetoelectric effect dubbed multiferroic order [1–3]. Usually, the largest magnetoelectric force is given by the exchange-striction. Spatial imbalance in the symmetric magnetic exchange leads to a lattice modulation. When it breaks the inversion symmetry, a finite net dipole moments appears as the ferroelectric polarization.

Recent observations of the ferroelectric polarization at the onset of the spiral magnetic order in TbMnO_3 [4–6] and $\text{Ni}_3\text{V}_2\text{O}_8$ [7] have attracted revived interests in multiferroic behavior from the viewpoints of the fundamental physics as well as applications [3]. Microscopic [8] and phenomenological [9, 10] theories have revealed that spiral and conical spin structures can couple to the polarization \mathbf{P} in the absence of any symmetry breaking through $\mathbf{P} \cdot \mathbf{J}_s$, where $\mathbf{J}_s \propto \mathbf{e} \times (\mathbf{S}_r \times \mathbf{S}_{r+e}) \propto \mathbf{S}(\nabla \cdot \mathbf{S}) - (\mathbf{S} \cdot \nabla)\mathbf{S}$ is the spin current produced between the two spins \mathbf{S}_r and \mathbf{S}_{r+e} at sites \mathbf{r} and $\mathbf{r} + \mathbf{e}$, respectively. This coupling has been derived by taking account of the spin-orbit coupling λ for a model of the t_{2g} orbitals of TM ions hybridized with the L p orbitals [8, 11], an e_g system coupled to the localized t_{2g} spin [12], and a sp hybridized model [13].

Effects of the exchange-striction and the Dzyaloshinskii-Moriya (DM) interaction have also been discussed in the context of the multiferroic RMnO_3 [14].

In view of the recent proliferation in the number of multiferroic materials, a proper classification scheme seems to be in order. In this Letter, we propose a systematic microscopic theory of the magnetically induced polarization and lattice modulation in multiferroic transition-metal oxides, by means of a strong-coupling expansion in both V/Δ and λ/Δ . We classify various microscopic mechanisms for the polarization and their distinct features. The classification scheme offers a way of identifying the material-specific mechanism by probing the magnetically induced non-uniform shifts of the L ions. As the specific demonstration, key experimental observations on the polarization and the lattice modulation in TbMnO_3 are analyzed.

Let us consider a cluster composed of TM ions at \mathbf{r} and $\mathbf{r} + \mathbf{e}$ hybridized through a L ion at the center $\mathbf{r} + \mathbf{e}/2$ as shown in Fig. 1 (a). For simplicity, we neglect a deviation of the bond angle away from 180° . The dipole moment $\mathbf{P}_{\mathbf{r}+\mathbf{e}/2}$ induced at the ligand site $\mathbf{r} + \mathbf{e}/2$ is generally expressed as

$$\begin{aligned} \mathbf{P}_{\mathbf{r}+\mathbf{e}/2} = & [P_{\mathbf{r},\mathbf{r}+\mathbf{e}}^{\text{nm}} + P_{\mathbf{r},\mathbf{r}+\mathbf{e}}^{\text{ms}}(\mathbf{m}_r \cdot \mathbf{m}_{r+\mathbf{e}})] \mathbf{e} \\ & + P_{\mathbf{r},\mathbf{r}+\mathbf{e}}^{\text{orb}} [(\mathbf{e} \cdot \mathbf{m}_r)\mathbf{m}_r - (\mathbf{e} \cdot \mathbf{m}_{r+\mathbf{e}})\mathbf{m}_{r+\mathbf{e}}] \\ & + P_{\mathbf{r},\mathbf{r}+\mathbf{e}}^{\text{sp}} \mathbf{e} \times (\mathbf{m}_r \times \mathbf{m}_{r+\mathbf{e}}) \end{aligned} \quad (1)$$

up to second order in the local spin moments \mathbf{m}_r and $\mathbf{m}_{r+\mathbf{e}}$. Here, $P^{\text{nm}} \propto V/\Delta$ is the nonmagnetic term that occurs regardless of the magnetic properties. $P^{\text{ms}} \propto (V/\Delta)^3$ represents the magnetostriction term. These effects do not demand the spin-orbit interaction. The orbital term $P^{\text{orb}} \sim \min(\lambda/V, 1)(V/\Delta)$ has been obtained

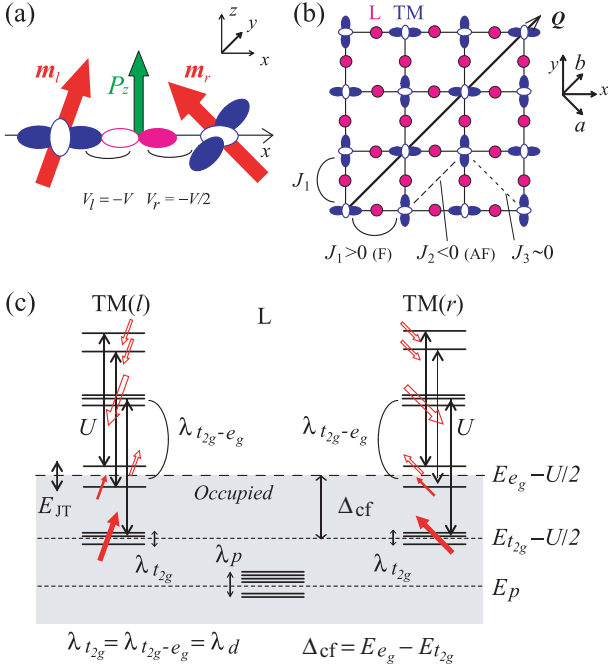


FIG. 1: (color online) (a) The TM-L-TM cluster model with the rod-type $d_{3x^2-r^2}/d_{3y^2-r^2}$ staggered orbital order under a noncollinear spin configuration with the associated electric polarization. (b) The lattice structure of the perovskite system within the xy (or ab) plane. The staggered orbital order for TbMnO_3 is also shown. (c) The level scheme for the $t_{2g}^3 e_g^1$ high-spin ($S = 2$) configuration.

in the study of partially filled degenerate t_{2g} orbitals[11]. Finally, the spin-current term $P^{\text{SP}} \propto (\lambda/\Delta)(V/\Delta)^3$ was demonstrated for the degenerate t_{2g} model [8, 11] and, as will be shown below, exists for any Mott-insulating electron configuration. P^{SP} and P^{orb} are *even* under the spatial inversion and found only in the presence of spin-orbit interaction, while P^{nm} and P^{ms} are *odd* and present only in the absence of the inversion symmetry.

On an array of $\dots\text{-TM-L-TM-L}\dots$ with (at most) two inequivalent L positions due to the orthorhombic distortion and/or staggered orbital order, the various mechanisms of polarization are manifested as Fourier harmonics in X-ray or neutron scattering probes. Assuming a general conical structure $\mathbf{m}_r = \mathbf{m}_0 + \mathbf{m}_1 \cos \mathbf{Q} \cdot \mathbf{r} - \mathbf{m}_2 \sin \mathbf{Q} \cdot \mathbf{r}$, we obtain the nontrivial Fourier components $\mathbf{P}(\mathbf{q}) = \sum_{\mathbf{r}, e} \mathbf{P}_{\mathbf{r}+e/2} e^{-i\mathbf{q} \cdot (\mathbf{r}+e/2)}$ shown in Table I, with $\mathbf{m}_\pm = \mathbf{m}_1 \pm i\mathbf{m}_2$ and $\mathbf{P}_{\mathbf{r}+e/2}$ given in Eq. (1). To compensate the electrostatic energy loss, each L ion tends to shift towards the induced dipole moment and cause the lattice modulation with the same wave vectors. P^{ms} gives a collinear lattice modulation along the cluster direction with wave vectors $\pi\mathbf{e} + \mathbf{Q}$ and $\pi\mathbf{e} + 2\mathbf{Q}$, where the shift of $\pi\mathbf{e}$ is due to the present of two equivalent L sites. It becomes uniform for the special case $\mathbf{Q} \cdot \mathbf{e} = \pi/2$, or period four for magnetism. This case is relevant for

$\mathbf{P}(\mathbf{q})$	Mechanisms	Polarization
$\mathbf{P}(0)$	P^{SP}	$-\mathbf{e} \times (\mathbf{m}_1 \times \mathbf{m}_2) \sin \mathbf{Q} \cdot \mathbf{e}$
$\mathbf{P}(\pm(\pi\mathbf{e} + \mathbf{Q}))$	P^{ms}	$\mathbf{e} [\mathbf{m}_0 \cdot (\mathbf{m}_1 \pm i\mathbf{m}_2)] \cos[\mathbf{Q} \cdot \mathbf{e}/2]$
$\mathbf{P}(\pm(\pi\mathbf{e} + 2\mathbf{Q}))$	P^{ms}	$\mathbf{e} (\mathbf{m}_1^2 + \mathbf{m}_2^2)/4$
$\mathbf{P}(\pm\mathbf{Q})$	P^{orb}	$\mp i [(\mathbf{e} \cdot \mathbf{m}_0) \mathbf{m}_\pm + (\mathbf{e} \cdot \mathbf{m}_\pm) \mathbf{m}_0]$
	P^{SP}	$\mp \frac{1}{2} \mathbf{e} \times (\mathbf{m}_0 \times \mathbf{m}_\mp) \sin[\mathbf{Q} \cdot \mathbf{e}/2]$
$\mathbf{P}(\pm 2\mathbf{Q})$	P^{orb}	$\mp \frac{1}{2} [(\mathbf{e} \cdot \mathbf{m}_\pm) \mathbf{m}_\pm] \sin \mathbf{Q} \cdot \mathbf{e}$

TABLE I: Wave vectors and directions of the lattice modulation originating from the mechanisms P^{ms} , P^{orb} , and P^{SP} . P^{nm} always gives a modulation with wave vector $\pi\mathbf{e}$.

HoMnO_3 as pointed out by Sergienko *et al.* recently[14]. Under the spiral (conical) magnetic structure, P^{orb} yields a spiral, even noncoplanar, modulation, while P^{SP} gives a uniform (conical) modulation. P^{orb} is found only in the unfulfilled t_{2g} system[11]. These results can be used to classify the mechanisms of the magnetoelectric couplings using X-ray and neutron scattering experiments.

Equation (1) can be derived from the TM-L-TM cluster model[8, 11] composed of the L p orbitals and the two TM d orbitals which are hybridized with L through the Slater-Koster parameters $V_{pd\sigma}$ and $V_{pd\pi}$. We assume an effective Zeeman field $(U/2)\hat{\mathbf{m}}_a$ ($a = l/r$ for the left/right TM ion) with an energy separation U , which originates from the local Coulomb repulsion and the Hund coupling in the magnetically ordered phase. The local energy levels of the TM d_α and L p orbitals are E_{d_α} and E_p , respectively, while the spin-orbit couplings for d and p orbitals are denoted λ_d and λ_p .

The mechanisms responsible for the spin-induced dipole moments through spin-orbit coupling can be classified as in Table II. Spin-orbit interaction $\lambda_{t_{2g}}$ within the degenerate t_{2g} manifold can be a source of polarization, P^{SP} and P^{orb} [8, 11], when the t_{2g} orbital degrees of freedom are unquenched, e.g. t_{2g}^n with $n = 1, 2, 4, 5$. It was derived in a previous paper [11] that P^{orb} and P^{SP} appear in proportion to $\min(\lambda_d/V_{pd\pi}, 1)(V_{pd\pi}/\Delta)$ and $(\lambda_d/\Delta)(V_{pd\pi}/\Delta)^3$, respectively, in the t_{2g}^5 configuration, where $\Delta = E_{t_{2g}} + U/2 - E_p$. The t_{2g}^2 configuration is related to t_{2g}^5 with the change in the charge transfer energy to $\Delta = E_{t_{2g}} - U/2 - E_p$, and the t_{2g}^1 to t_{2g}^4 in the same manner. Another symmetry operation can be used to show that P^{SP} and P^{orb} for t_{2g}^4 is related to those of t_{2g}^5 by a sign change, as well as those for t_{2g}^1 to t_{2g}^2 . Due to the strong Hund coupling, the t_{2g}^3 and t_{2g}^6 configurations represent the orbital quenched case with no polarization arising from orbital deformation.

The spin-orbit interaction within the e_g manifold vanishes and has no impact on spin-polarization coupling. In this case, the spin-orbit interaction λ_p at the ligand oxygen site can mediate the spin-polarization coupling P^{SP} , as we demonstrate below. In addition, mixing of an occupied e_g level and an unoccupied t_{2g} , or of an unoccupied e_g and an occupied t_{2g} , can occur due to the spin-orbit

Spin-orbit	Configuration	Polarization
$\lambda_{t_{2g}}$	t_{2g}^n ($n = 1, 2, 4, 5$)	$P^{\text{SP}}, P^{\text{orb}}$
$\lambda_{t_{2g}-e_g}$	arbitrary d^n , nonzero S	P^{SP}
λ_p	arbitrary d^n , nonzero S	P^{SP}

TABLE II: Classification of the spin-orbit interactions and the corresponding types of induced polarization and the relevant d electron configuration. Nonzero net magnetic moment for the d electrons, $S \neq 0$, is required to generate magnetic ground states. $\lambda_{t_{2g}-e_g}$ (λ_p) effects decrease (increase) as the electron number n increases.

interaction $\lambda_{t_{2g}-e_g}$ in the given TM ion and contribute to the polarization P^{SP} . Such mechanism was demonstrated for TbMnO₃ recently[12]. Both mechanisms described in this paragraph should apply for arbitrary d^n configuration, as long as the net magnetic moment remains nonzero to guarantee magnetic ordering.

A low- n transition metal involving Ti or V will be the likely candidate to observe t_{2g} -mediated P^{SP} and P^{orb} . A spin-canted phase in YVO₃ was found recently[15]. For such a state we argue that P^{orb} , which is much larger than P^{SP} on the atomic scale, is detectable in the microscopic X-ray or neutron probes. The specific dependence of P^{orb} on the local magnetic structure given in Eq. (1) and in Table I can be checked experimentally.

Recently, a number of e_g systems with filled t_{2g} came to be classified as a multiferroic: a nickelate Ni₃V₂O₈ [7] with d^8 , and a cuprate LiCuVO₄ [18] with d^9 . We propose that the oxygen spin-orbit-mediated mechanism should play an important role for these materials. For instance, the d^9 Cu sites can be modeled as $d_{x^2-y^2}$ orbitals at the TM sites in the cluster model. Taking $-V_l = V_r = V_{pd\sigma}$ [16], P^{SP} is given by[17]

$$P_{\lambda_p}^{\text{SP}} = -2\sqrt{2}(L_{r,z} + L_{l,z})\frac{\lambda_p}{\Delta}\left(\frac{V_{pd\sigma}}{\Delta}\right)^3 \quad (2)$$

where $\Delta = E_{e_g} + U/2 - E_p$, and E_{e_g} is the energy of the relevant e_g orbital. Here $L_{a,z}$ denotes the integral $L_{a,z} = \langle d_a | z | p_z \rangle$ with $a = r, l$. The d^8 contains two e_g orbitals with $S = 1$, that can be decomposed as $d_{3x^2-r^2}$ and $d_{y^2-z^2}$ in the degenerate case. Of these, the latter does not couple to the oxygen orbitals and one is left with a single $d_{3x^2-r^2}$ orbital per site with the polarization again given by Eq. (2). No P^{orb} term is found for pure e_g models with oxygen spin-orbit interaction.

The d^7 case with a single e_g electron is subject to the Jahn-Teller distortion and the lifting of the orbital degeneracy. When the same e_g orbitals are occupied for the adjacent TM sites, one again has Eq. (2). If not, the appropriate cluster model should involve different orbitals for the right and left TM's, and the inversion symmetry breaking yields non-zero values of

$$P^{\text{nm}} = (L_{r,x} - L_{l,x})\frac{V_{pd\sigma}}{\Delta}, \quad P^{\text{ms}} = \frac{1}{4}(L_{l,x} - L_{r,x})\left(\frac{V_{pd\sigma}}{\Delta}\right)^3, \quad (3)$$

with $L_{a,x} = \langle d_a | x | p_x \rangle$. On the local scale both terms, being independent of spin-orbit interaction, are greater than $P_{\lambda_p}^{\text{SP}}$. Except for special circumstances, however, P^{nm} and P^{ms} are finite- \mathbf{q} modulations with zero macroscopic average. Even for the d^9 and d^8 cases, the orthorhombic distortion displaces the oxygen position away from the middle of the TM ions, then one has the appearance of Eq. (3) in the polarization.

As a concrete example of the $\lambda_{t_{2g}-e_g}$ mechanism at work, we discuss the case of $t_{2g}^3 e_g^1$ configuration found in TbMnO₃ with Mn³⁺ ion. Because of the large Jahn-Teller effect, TbMnO₃ exhibits the rod-type $d_{3x^2-r^2}/d_{3y^2-r^2}$ orbital ordering shown in Fig. 1(b) far above the room temperature[19]. Accordingly we assume that the $d_{3x^2-r^2}$ and $d_{3y^2-r^2}$ orbitals are occupied at the l and r sites of the TM-L-TM cluster. Assuming $V_l = V_r = -V_{pd\sigma}$, one obtains polarization of the spin-current form[17]

$$P_{t_{2g}-e_g}^{\text{SP}} = -\sqrt{3}L'_z\frac{\lambda_d}{U - \Delta_{cf} + E_{JT}/2}\left(\frac{V_{pd\sigma}}{\Delta}\right)^3 \quad (4)$$

where Δ_{cf} is the crystal field gap $E_{e_g} - E_{t_{2g}}$, E_{JT} is the Jahn-Teller energy splitting, and $L'_z = \langle d_{l,zx} | z | p_x \rangle = \langle d_{r,zx} | z | p_x \rangle$ [12, 17]. A similar term is obtained for uniform orbital order, i.e. same d -orbitals for both TM ions in the cluster. No orbital polarization P^{orb} is induced from the mixing[17].

In the rest of the paper, we compare the experimental situation with the theoretical analysis for TbMnO₃, which probably presents the most complex situation with orbital ordering, unfulfilled t_{2g} and e_g levels, and $t_{2g}-e_g$ mixing. The two terms, Eq. (4) and Eq. (2), combine constructively to produce P^{SP} , the uniform polarization. Quantitative agreement with the measured uniform polarization value in TbMnO₃ is obtained as follows.

Matrix elements needed to evaluate Eq. (2) and Eq. (4) are calculated by taking the TM-O bond length 1.9Å and the Clementi-Raimondi effective charges [21] $Z_{\text{Mn}3d}^{\text{eff}} = 10.53$ and $Z_{\text{O}2p}^{\text{eff}} = 4.45$. Other parameters are chosen as $V_l = 2V_r = -V_{pd\sigma} = -1.2$ eV, $U = 3$ eV and $E_{e_g} - E_p = 2$ eV. The spin-orbit coupling for the oxygen $2p$ and TM $3d$ orbitals are chosen from $\lambda_L \equiv 2\Delta E_L/(2L + 1)$, where $L = 1, 2$ for p and d orbitals. The spin-orbit energy splitting is given by $\Delta E_p = 37$ meV ($\lambda_p = 25$ meV), and $\Delta E_d = 120$ meV ($\lambda_d = 48$ meV), respectively[20]. With these values we obtain the uniform polarization along the c axis $P_{\lambda_p}^{\text{SP}} \sim 130$ $\mu\text{C}/\text{m}^2$ from the oxygen spin-orbit interaction, and $P_{t_{2g}-e_g}^{\text{SP}} \sim 860$ $\mu\text{C}/\text{m}^2$ from the $t_{2g}-e_g$ mixing with $\Delta_{cf} = 2$ eV and $E_{JT} = 1$ eV. The net value $P^{\text{SP}} \sim 990$ $\mu\text{C}/\text{m}^2$ multiplied

with $|\mathbf{m}_r \times \mathbf{m}_{r+e}| \approx \sin(0.28\pi)$ in Eq. (1) gives the uniform c -axis polarization of $\sim 760 \mu\text{C}/\text{m}^2$, in reasonable agreement with the experimental value in TbMnO_3 [4, 5] ($\sim 700 \mu\text{C}/\text{m}^2$ at 10K). The direction of the polarization is also consistent with the experiment.

The X-ray intensity of the $2Q$ lattice modulation in TbMnO_3 increases monotonically between the Neel temperature T_N for the collinear magnetic phase, and T_L , the latter signaling the onset of ferroelectricity, as the temperature is lowered. Then the signal decreases with lower temperature in the non-collinear, ferroelectric phase, $T < T_L$. Both features can be understood by taking the view that the non-uniform component arises from the magnetostriction term, due to the breaking of the inversion symmetry in each TM-L-TM cluster from the orbital ordering and the orthorhombic distortion.

The spin configuration in the magnetic phase $T < T_N$ can be described by the ordered spin moment, $\langle \mathbf{s}_i \rangle = S(\hat{b} \cos \theta_i + \hat{c} \sqrt{1 - e^2} \sin \theta_i)$. It evolves from collinear ($e = 1$) to nearly circular ($e = 0$) pattern with decreasing temperature [6]. In the collinear phase, one has $e = 1$ while the magnitude S increases monotonically at the lower temperature. The TM-L-TM cluster calculation can be generalized to handle these cases, both collinear and elliptic, by writing a self-consistent equation $\langle \mathbf{s}_i \rangle = \frac{\int d\Omega_i \mathbf{m}_i w_i}{\int d\Omega_i w_i}$ with a weight $w_i = \exp[\beta_i \langle \mathbf{s}_i \rangle \cdot \mathbf{m}_i]$.

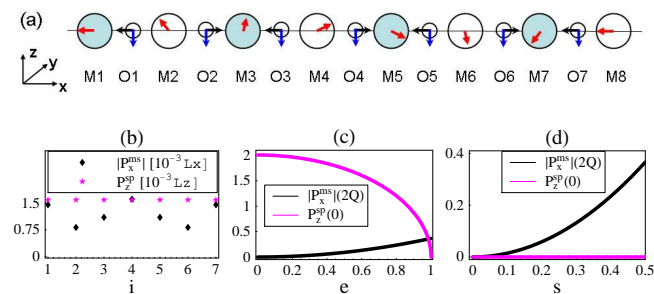


FIG. 2: (color online) (a) Elliptical spiral spins (red arrows) with the ellipticity $e = 0.6$ and the associated local dipole moments arising from oxygen spin-orbit interaction are shown as P_z^{SP} (blue arrows, enlarged by 10^3 times) and P_x^{MS} (black arrows) for the observed spin modulation period ($Q \approx 0.28\pi$) as in TbMnO_3 at low temperature. Two types of Mn sites exist (blue and white) due to orbital ordering. Statistical weights are introduced to account for elliptical spins. P_x^{MS} alternates its direction due to staggered orbital order. (b) Induced dipole moments $P_{z,i}^{\text{SP}}$ and $|P_{x,i}^{\text{MS}}|$ at the oxygen site O_i in $\text{TM}_i\text{-}O_i\text{-}\text{TM}_{i+1}$ cluster in units of $10^{-3}L_z$ and $10^{-3}L_x$, respectively, and $L_{z(x)}$ is defined by $L_{l,z(x)}$. (c,d) Main Fourier components of the dipole moments, at $q = 2Q$ for $|P_{x,i}^{\text{MS}}|$ and at $q = 0$ for $P_{z,i}^{\text{SP}}$, as functions of e for $T < T_L$ in (c) and S with $e = 1$ for $T_L < T < T_N$ in (d). Note that e in (c) and $1/2 - S$ in (d) decrease with lowering temperature. This figure is worked out for the orbital ordered model of TbMnO_3 (Figs. 1) with $(U, \Delta_{cf}, E_{JT}, V_{pd\sigma}, \lambda_p, \lambda_d) = (3.0, 2.0, 1, 1.2, 0.025, 0.048) \text{ eV}$.

Average over the $O(3)$ vector \mathbf{m}_i determines the appropriate β_i . The dipole moment in the collinear/elliptic spin configuration can be obtained by taking the average of Eq. (1) over the spins \mathbf{m}_r and \mathbf{m}_{r+e} with weights w_r and w_{r+e} , for the magnetic period $\sim 0.28\pi$ configuration of the low-temperature TbMnO_3 .

As shown in Fig. 2 (d), in the collinear phase, ($e = 1$), the $2Q$ intensity arising from the magnetostriction P^{MS} monotonously increases with the ordered spin amplitude S . Then in the non-collinear phase ($e < 1$), the $2Q$ intensity arising from P^{MS} decreases for smaller e corresponding to a lower temperature (Fig. 2 (c)). The direction of the lattice modulation in TbMnO_3 has not been clearly determined yet [22]. A proper identification of the lattice modulation direction in the future can be used to discriminate the different scenarios of magneto-electric coupling.

The authors acknowledge fruitful discussion with T. Arima, Y. Tokura, F. Ishii, and T. Ozaki. H. J. H. was supported by the Korea Research Foundation through Grant No. KRF-2005-070-C00044. The work was partly supported by the Grant-in-Aids from under the Grant No. 15104006, 16076205, and 17105002, and NAREGI Nanoscience Project from the Ministry of Education, Culture, Sports, Science, and Technology, Japan.

* Electronic address: cljia@kias.re.kr

† Electronic address: onoda@sss1.t.u-tokyo.ac.jp

‡ Electronic address: nagaosa@ap.t.u-tokyo.ac.jp

§ Electronic address: hanjh@skku.edu

- [1] P. Curie, *J. Phys.* **3**, 393 (1894).
- [2] M. Fiebig, *J. Phys. D: Appl. Phys.* **38**, R123 (2005).
- [3] Y. Tokura, *Science* **312**, 1481 (2006).
- [4] T. Kimura *et al.* *Nature* **426**, 55 (2003).
- [5] M. Kenzelmann *et al.* *Phys. Rev. Lett.* **95**, 087206 (2005).
- [6] T. Arima *et al.* *Phys. Rev. Lett.* **96**, 07202 (2006).
- [7] G. Lawes, *et al.* *Phys. Rev. Lett.* **95**, 087205 (2005).
- [8] H. Katsura, N. Nagaosa, and A.V. Balatsky, *Phys. Rev. Lett.* **95**, 057205 (2005).
- [9] M. Mostovoy, *Phys. Rev. Lett.* **96**, 067601 (2006).
- [10] A. B. Harris and G. Lawes, cond-mat/0508617; A. B. Harris, cond-mat/0508730; A. B. Harris, T. Yildirim, A. Aharony, and O. Entin-Wohlman, cond-mat/0510807.
- [11] C. Jia, S. Onoda, N. Nagaosa, and J. H. Han, *Phys. Rev. B* **74**, 224444 (2006).
- [12] C. D. Hu, cond-mat/0608470.
- [13] T. A. Kaplan and S. D. Mahanti, unpublished.
- [14] I. A. Sergienko and E. Dagotto, *Phys. Rev. B* **73**, 094434 (2006). I. A. Sergienko, C. Sen and E. Dagotto, *Phys. Rev. Lett.* **97**, 227204 (2006).
- [15] Y. Ren *et al.* *Nature* **396**, 441 (1998).
- [16] For $V_l = V_r = -V_{pd\sigma}$ one has to replace $L_{r,z(x)}$ with its negative value. Generic expressions for arbitrary V_l and V_r are not available.
- [17] Details will be published elsewhere.
- [18] Y. Naito *et al.*, cond-mat/0611659.
- [19] T. Kimura *et al.* *Phys. Rev. B* **68**, 060403(R) (2006).

- [20] S. Kotochigova *et al*, Phys. Rev. A **55**, 191 (1997); *ibid.* **56**, 5191 (1997).
- [21] E. Clementi and D. L. Raimondi, J. Chem. Phys. **38**, 2686 (1963); E. Clementi, D. L. Raimondi, and W.P. Reinhardt, J. Chem. Phys. **47**, 1300 (1967).
- [22] T. Arima, private communications.